Silicon microring carrier-injection-based modulators/switches with tunable extinction ratios and OR-logic switching by using waveguide cross-coupling

Chao Li, Linjie Zhou, and Andrew W. Poon

Photonic Device Laboratory, Department of Electronic and Computer Engineering, The Hong Kong University of Science and Technology, Clear Water Bay, Hong Kong SAR, China
eeawpoon@ust.hk

Abstract: We demonstrate silicon microring carrier-injection-based modulators/switches with waveguide cross-coupling. We tune the modulator extinction ratio by forward-biasing either the microring or cross-coupled waveguide p-i-n diode, while modulating the other. We also demonstrate OR-logic switching functionality by simultaneously applying two different electrical data streams across the microring and cross-coupled waveguide diodes. For both the modulator and the switch, we observe NRZ pattern-dependent optical waveform distortions.

OCIS codes: (250.7360) Waveguide modulators; (250.5300) Photonic integrated circuits; (230.5750) Resonators.

References and links

1. I. Kiyat, A. Aydinli, and N. Dagli, "Low-power thermooptical tuning of SOI resonator switch," IEEE Photon. Technol. Lett. **18**, 364-366 (2006).
2. G. N. Nielson, D. Seneviratne, F. Lopez-Royo, P. T. Rakich, Y. Avrahami, M. R. Watts, H. A. Haus, H. L. Tuller, and G. Barbastathis, "Integrated wavelength-selective optical MEMS switching using ring resonator filters," IEEE Photon. Technol. Lett. **17**, 1190-1192 (2005).
3. V. R. Almeida, C. A. Barrios, R. R. Panepucci, and M. Lipson, "All-optical control of light on a silicon chip," Nature **431**, 1081-1084 (2004).
4. Q. Xu, B. Schmidt, S. Pradhan, and M. Lipson, "Micrometre-scale silicon electro-optic modulator," Nature **435**, 325-327 (2005).
5. M. Lipson, "Compact Electro-Optic Modulators on a Silicon Chip," IEEE J. Selected Topics in Quantum Electron, **12**, 1520-1526 (2006)
6. Q. Xu, S. Manipatruni, B. Schmidt, J. Shakya, and M. Lipson, "12.5 Gbit/s carrier-injection-based silicon micro-ring silicon modulators," Opt. Express **15**, 430-436 (2007).
7. C. Gunn, "CMOS photonics technology platform," invited paper 6125-01, *SPIE Photonics West*, SPIE Proceedings **6125** on Silicon Photonics, San Jose, CA, 25 Jan 2006.
8. R. A. Soref and B. R. Bennett, "Electrooptical effects in silicon," IEEE J. Quantum Electron. **QE-23**, 123-129 (1987).
9. L. Zhou and A. W. Poon, "Silicon electro-optic modulators using p-i-n diodes embedded 10-micron-diameter microdisk resonators," Opt. Express **14**, 6851-6857 (2006).
10. S. Mookherjea, "Mode cycling in microring optical resonators," Opt. Lett. **30**, 2751-2753 (2005).
11. W. Green, R. Lee, G. DeRose, A. Scherer, and A. Yariv, "Hybrid InGaAsP-InP Mach-Zehnder Racetrack Resonator for Thermooptic Switching and Coupling Control," Opt. Express **13**, 1651-1659 (2005).
12. L. Zhou and A. W. Poon, "Silicon electro-optics switches using microring resonators with phase-tunable feedback," in *proceedings of IEEE/LEOS 3rd International Conference on Group IV Photonics*, Ottawa, Canada, Sep. 13-15, 2006.

1. Introduction

Silicon microresonator-based modulators/switches that are CMOS-compatible and micrometer-scale in size have recently been demonstrated and attracting considerable academic and industrial research interest [1-7]. Among these, microresonator devices using

#80360 - $15.00 USD Received 22 Feb 2007; revised 9 Apr 2007; accepted 10 Apr 2007; published 11 Apr 2007

free-carrier-plasma-dispersion [8] based electro-optic (EO) effect are particularly promising as they demonstrated beyond-GHz-speed switching [4-7], and offer the prospect of compact optoelectronic integrated circuits (OEICs) with CMOS circuits on the silicon substrate. Specifically, Xu et al. in their pioneering work [4] demonstrated GHz-speed carrier-injection-based silicon microring modulators using laterally integrated p-i-n diodes. Most recently, Xu et al. [6] has further demonstrated their silicon microring EO modulators up to 12.5 Gbps. On the industry end, Luxtera Inc. [7] reported in year 2006 10-Gbps microring EO modulators using laterally integrated depletion-type p-n diode. Previously, our research group also demonstrated a 10-micrometer-sized silicon microdisk carrier-injection-based EO modulator using selectively integrated p-i-n diodes, with 3-dB bandwidth up to ~500 MHz [9].

In order to advance the functionality of microresonator modulators/switches, it is desirable to enable further active control on the resonance characteristics. Recently, several research groups [10-12] have investigated resonance control by means of waveguide cross-coupling to the microresonator, in which the cross-coupled waveguide essentially acts as an external feedback to the microresonator. Compared with the conventional microresonator notch filter configuration which only has a single waveguide coupling region, the cross-coupling configuration enables controlled resonance wavelength and extinction ratio (ER) tuning by phase-shifting the cross-coupled waveguide (instead of directly tuning the microresonator). The waveguide-cross-coupled-microresonator also imposes a different resonance phase-matching condition from the conventional single-waveguide-coupled-microresonator. The cross-coupling is expected to be more sensitive to phase changes, and thus potentially provides more efficient microresonator modulators/switches.

Here we report silicon microring carrier-injection-based EO modulators and switches with waveguide cross-coupling. Due to the waveguide cross-coupling, the resonance wavelength and ER can be electrically tuned by forward-biasing either the microring or cross-coupled waveguide p-i-n diodes. We also demonstrate electrical OR-logic switching functionality in the optical transmission by simultaneously driving both the microring and cross-coupled waveguide diodes with different data streams.

2. Device design and principle

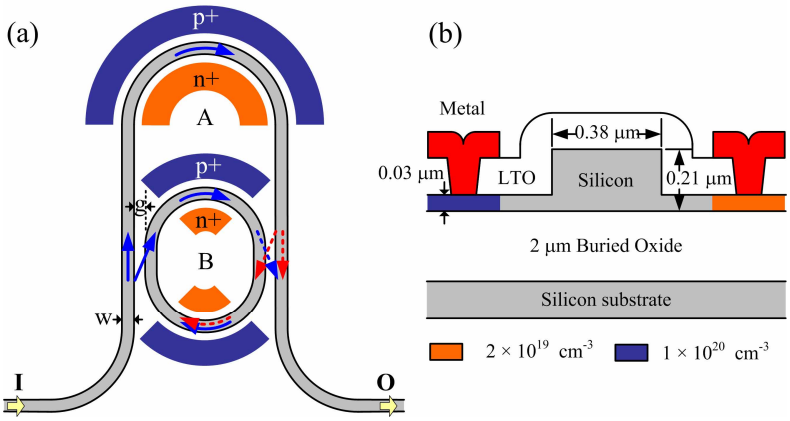

Fig. 1. (a). Schematic of the microring EO modulator/switch with waveguide cross-coupling. Two terminals of p-i-n diodes are laterally integrated to the U-bend waveguide (node *A*) and the microring arcs (node *B*). The arrows indicate the lightwave propagation and the coupling in the cross-coupled microring. I: Input; O: Output. w: waveguide width; g: gap separation between the waveguide and the coupled microring. (b). Cross-sectional schematic of the p-i-n diode. LTO: low-temperature oxide

Figure 1(a) depicts a schematic of the microring EO modulator/switch with waveguide cross-coupling. The device reported here is based on our previous work on silicon microring notch filters comprising a racetrack microring that is double-coupled (cross-coupled) to a single-mode U-bend waveguide [12]. The phase-matching condition is strongly dependent on the

#80360 - $15.00 USD Received 22 Feb 2007; revised 9 Apr 2007; accepted 10 Apr 2007; published 11 Apr 2007

cross-coupling-induced feedback, and thereby the resonance characteristics are distinct from those of single microresonators. We remark that under various feedback amplitudes and phases, some resonances are near critically coupled while some resonances are nearly suppressed. One p-i-n diode (node *A*) is laterally integrated across the U-bend waveguide and two other p-i-n diodes (node *B*) of the same structure as node *A* are laterally integrated across two arcs of the microring. Thus, biasing node *A* (with voltage V_A) phase-shifts the cross-coupled waveguide, whereas biasing node *B* (with voltage V_B) phase-shifts the microring. We note that both nodes *A* and *B* can be used for biasing or signal modulation. As modulators, forward-biasing one of the nodes tunes the microring resonance wavelength and ER. As switches, we can simultaneously input electrical data streams as driving signals to both nodes. Figure 1(b) shows the cross-sectional schematic of the embedded p-i-n diode.

3. Device fabrication

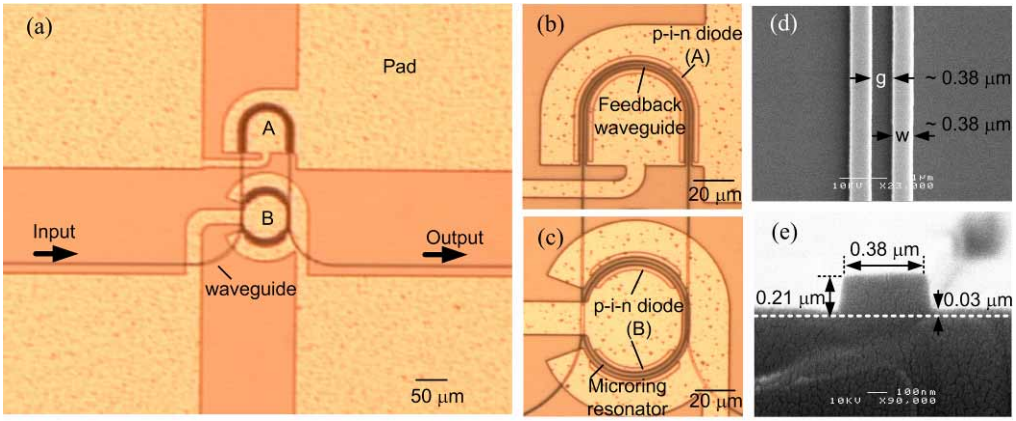

Fig. 2. (a). Top-view optical micrograph of the fabricated device on a silicon chip. (b), (c) Zoom-in view optical micrographs of the two embedded p-i-n diodes along the U-bend (feedback) waveguide (node *A*) and along the microring arcs (node *B*). (d) Scanning electron micrograph (SEM) of the waveguide-resonator coupling region without the oxide upper-cladding. g ~ 0.38 μm, w ~ 0.38 μm. (e) SEM cross-sectional view of the single-mode waveguide without the oxide upper-cladding.

We employ standard silicon nanofabrication processes as in our previous work [9]. We use commercial silicon-on-insulator (SOI) wafers with a 0.55-μm device layer on top of a 2-μm buried oxide (BOX) layer for the device fabrication. In order to enhance the lateral coupling between the submicrometer-sized rib waveguide and the microring over a relatively wide coupling gap, we use wet-oxidation to thin-down the top silicon layer to a desired 0.21-μm-thick device layer with a smooth top surface. The device layout is defined by photolithography (i-line, 0.365 μm), and transferred onto the device layer by CF_4-based plasma etching. We implant phosphorous (concentration of 1×10^{20} cm^{-3}) and boron (2×10^{19} cm^{-3}) dopants to form the n^+ and p^+-doped regions. The entire device is clad with a 0.6-μm-thick low-temperature oxide (LTO) as an electrical isolation layer. After opening contact holes, a 0.7-μm-thick aluminum layer is sputtered and patterned for electrical connection. Figure 2(a) shows the top-view optical micrograph of the fabricated device. The racetrack microring arc radius is 25 μm, and the straight interaction length is 10 μm. The U-bend waveguide is ~280-μm-long measured between the mid-points of the racetrack straight interaction regions. There are a total of four metal pads in order to separately bias the two sets of p-i-n diodes. Figures 2(b) and 2(c) show the zoom-in view optical micrographs of the two p-i-n diodes integrated across the U-bend waveguide and the microring. The p-i-n diode integrated across the U-bend waveguide is ~135-μm-long, whereas the p-i-n diode integrated across each of the microring arcs is ~59-μm-long. Figure 2(d) shows the zoom-in view

#80360 - $15.00 USD Received 22 Feb 2007; revised 9 Apr 2007; accepted 10 Apr 2007; published 11 Apr 2007

scanning electron micrograph (SEM) of the waveguide-microring coupling region without the oxide cladding. The measured waveguide width and the coupling gap separation are both ~0.38 μm. Figure 2(e) shows the cross-sectional view SEM of the single-mode waveguide. The rib waveguide height is 0.21 μm with an etched depth of 0.18 μm. The p^+- and n^+-doped regions are positioned in the 0.03 μm slab layer, with ~0.5-μm separations from the waveguide sidewalls. We note that such heavily doped 0.03-μm slab layer may result in a moderate resistance, and hence a moderate RC time constant.

4. Modulators with tunable extinction ratios

Here we demonstrate a silicon microring EO modulator with ER actively tuned by means of waveguide cross-coupling. We electro-optically tune the resonance wavelength and ER by forward-biasing either the p-i-n diode across the U-bend waveguide or that across the microring, while modulating the other.

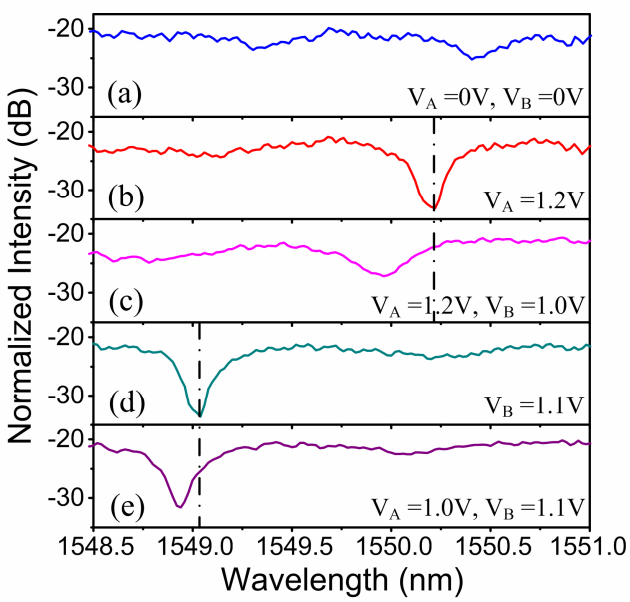

Fig. 3. Measured TE-polarized transmission spectra under various DC-bias voltages. (a) V_A = V_B = 0 V (blue line), (b) V_A = 1.2 V, V_B = 0 V (red line), (c) V_A = 1.2 V, V_B = 1.0 V (pink line), (d) V_A = 0 V, V_B = 1.1 V (green line), and (e) V_A = 1.0 V, V_B = 1.1 V (purple line).

Figures 3(a)–3(e) show the measured TE-polarized (electric field parallel to the chip) transmission spectra under various DC forward-biases of (a) V_A = V_B = 0 V, (b) V_A = 1.2 V, V_B = 0 V, (c) V_A = 1.2 V, V_B = 1.0 V, (d) V_A = 0 V, V_B = 1.1 V, and (e) V_A = 1.0 V, V_B = 1.1 V. Here we choose a nearly suppressed resonance, with an ER of only ~4 dB (at ~1550.4 nm), when both nodes *A* and *B* are un-biased. As we forward-bias node *A* only, the resonance becomes better coupled with a slight spectral blueshift until reaching a maximum ER of ~12 dB upon V_A = 1.2 V (at ~1550.2 nm). We attribute this observed maximum ER to critical coupling between the microring and the phase-shifted cross-coupled waveguide.

In the case of forward-biasing both nodes *A* (V_A = 1.2 V) and *B* (V_B = 1.0 V), we find that the resonance becomes moderately suppressed and blueshifts by ~0.24 nm from that upon V_A = 1.2 V only. At a probe wavelength of 1550.2 nm (labeled by a dashed-dotted line), the resultant intensity modulation between the two cases is ~11 dB.

In contrast, as we forward-bias node *B* only with V_B = 1.1 V, the resonance wavelength blueshifts by exceeding 1 nm (at ~1549.1 nm) with an enhanced ER of ~13 dB in comparison

#80360 - $15.00 USD Received 22 Feb 2007; revised 9 Apr 2007; accepted 10 Apr 2007; published 11 Apr 2007

with the unbiased case. We note that biasing node *B* phase-shifts the microring and thus significantly blueshifts the resonance.

In the case of forward-biasing both nodes *B* (V_B = 1.1 V) and *A* (V_A = 1.0 V), we find that the resonance is only slightly suppressed and only blueshifts by ~0.1 nm from that upon V_B = 1.1 V only. At a probe wavelength of 1549.1 nm (labeled by a dashed-dotted line), the resultant intensity modulation between the two cases is ~8.3 dB.

In order to examine the modulator response with a reasonable data rate, we apply a 200-Mbps NRZ electrical driving signal with ±1-V signal levels [shown in Fig. 4(a)] across node *B* while biasing node *A*, and launching a continuous-wave probe with wavelength in the vicinity of the resonance. The NRZ bit sequence is "01011101". Figure 4(b) shows the modulated optical waveform for V_A = 0 V. We observe only ~55% modulation depth which is consistent with the measured ER of ~4 dB [see Fig. 3(a)]. Figure 4(c) shows the modulated optical waveform for V_A = 1.2 V. The modulation depth is improved to ~90%, which is consistent with the intensity modulation of ~11 dB with DC biasing [see Figs. 3(b) and 3(c)].

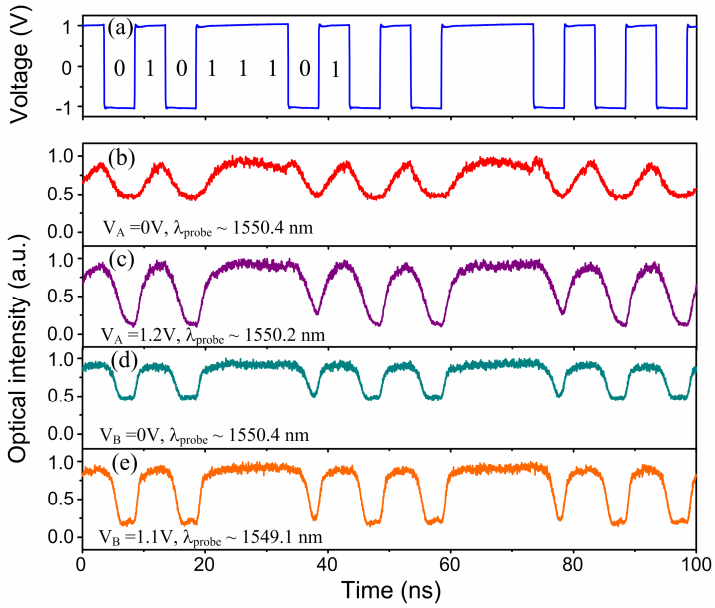

Fig. 4. (a). 200-Mbps NRZ electrical input data stream with ±1-V signal levels applied across node *A* or *B*. (b), (c) Measured optical waveforms upon node *B* modulation at a probe wavelength in the vicinity of the resonance under (b) V_A = 0 V, and (c) V_A = 1.2 V. (d), (e) Measured optical waveforms upon node *A* modulation at a probe wavelength in the vicinity of the resonance under (d) V_B = 0 V, and (e) V_B = 1.1 V.

Similarly, we forward-bias node *B* and modulate node *A* by applying the electrical driving signal. Figure 4(d) shows the modulated optical waveform for V_B = 0 V. We observe only ~50% modulation depth. Figure 4(e) shows the modulated optical waveform for V_B = 1.1 V. The modulation depth is improved to ~85%, which is consistent with the intensity modulation of ~8.3 dB with DC biasing [see Figs. 3(d) and 3(e)].

We remark that the optical waveforms from node *A* modulation exhibit sharper transitions than those from node *B* modulation. We attribute this in part to relatively less free-carriers diffusion escape near the two ends of the long U-bend waveguide diode. Thus, most of the free-carriers can be swept out upon the reverse-bias cycles. In contrast, modulating the relatively short arcs of the microring allows more carriers to escape by diffusion, and thereby slowing down the modulation [4, 5]. We measure the 3-dB bandwidth for both nodes A and B to be around 0.9 GHz. We attribute the bandwidth limitations to both the device design and the relatively low drive voltage. We believe that the relatively wide intrinsic regions (~1.4

#80360 - $15.00 USD Received 22 Feb 2007; revised 9 Apr 2007; accepted 10 Apr 2007; published 11 Apr 2007

μm) of the p-i-n diodes limits the rise times, while the carriers surface recombination lifetimes (~ ns) outside the p-i-n diodes limits the fall times.

Moreover, we observe pattern-dependent waveform distortions in which the ER varies with the length of the injection time. Such distortions are shown to be more significant with modulating node *B*. For example, in Fig. 4(c), we observe less ER (~5.6 dB) following three consecutive "1"s. Whereas, the ER is ~9.5 dB following a single bit "1". However, the fall times are not significantly different between the above two cases. We attribute the bit-pattern dependence to the accumulation of free-carriers after a long injection time, and the accumulated carriers in the intrinsic waveguide/microring regions cannot be completely swept out under the reverse-bias. Thus, the residual carriers slightly blueshift the resonance wavelength, resulting in a slightly increased transmission. In addition, the longer is the injection time, the more likely it is for the carriers to laterally diffuse outside the p-i-n diodes. Thus, we generally observe less ER's following consecutive "1"s [5].

5. OR-logic switching

Here we demonstrate silicon microring electrical-control logic switches using the same device with dual electrical inputs

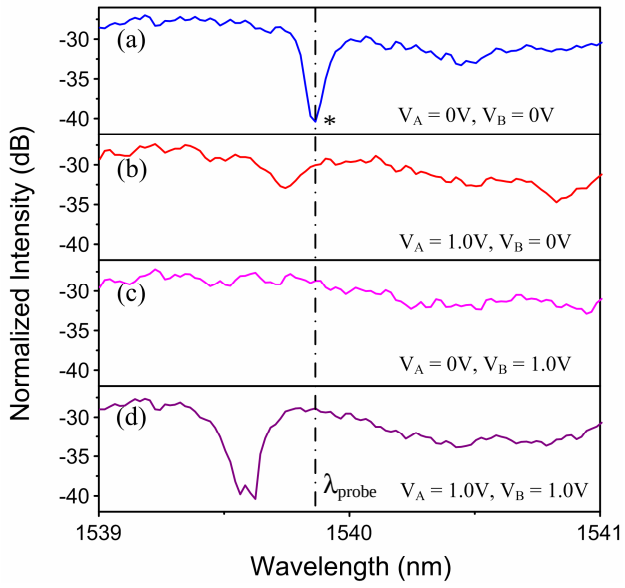

Fig. 5. Measured TE-polarized transmission spectra of the cross-coupled microring device with dual electrical inputs for four electrical signal input states (V_A, V_B) of (a) (0 V, 0 V), (b) (1.0 V, 0 V), (c) (0 V, 1.0 V), and (d) (1.0 V, 1.0 V). λ_{probe}: probe wavelength.

Figures 5(a)–(d) show the measured TE-polarized transmission spectra for four electrical signal input states (V_A, V_B) of (0 V, 0 V), (1.0 V, 0 V), (0 V, 1.0 V), and (1.0 V, 1.0 V). The resonance "*" displays a Q of ~9,000 (linewidth of ~0.17 nm) and an ER of ~12 dB. Here we choose a near critically coupled resonance when both nodes *A* and *B* are un-biased. The resonance is significantly suppressed when only node *A* is switched on (phase-shifting the cross-coupled waveguide), and totally suppressed when only node *B* is switched on (phase-shifting the microring). When both nodes *A* and *B* are switched on, the resonance reappears with a spectral blueshift of ~0.25 nm, an enhanced ER of ~12.8 dB, and a broadened linewidth of ~0.24 nm. The blueshifted resonance displays two unresolved dips and thus the resonance is inhomogeneously broadened.

At a probe wavelength in the vicinity of the resonance "*", the optical signal level varies between a high-level [Figs. 5(b)–(d)] and a low-level [Fig. 5(a)] upon different electrical

#80360 - $15.00 USD Received 22 Feb 2007; revised 9 Apr 2007; accepted 10 Apr 2007; published 11 Apr 2007

signal input states. Thus, when two electrical data streams are simultaneously applied across nodes *A* and *B*, the electrical states effectively impose logic-control functionality onto the optical transmission near a microring resonance.

Figures 6(a)-6(c) present the measured electrical-control temporal logic switching using the cross-coupled microring. We apply two different 200-Mbps NRZ electrical data streams with ±1-V signal levels across nodes *A* and *B* [Figs. 6(a) and 6(b)]. The dual input states span all possible binary combinations. Figure 6(c) shows the measured optical transmission waveform which exhibits OR-logic switching, with pattern-dependent optical waveform distortions. We observe a maximum ER of ~12 dB between the optical "1" and "0" levels, consistent with the ER observed in the measured spectra under DC-biasing (Fig. 5). The optical high-level of the (1, 1) state exceeds that of the (1, 0) state (~1.2 dB higher). We attribute this to the less spectral blueshift with the (1, 0) state as compared with the (1, 1) state [see Figs. 5(b) and 5(d)]. However, the optical high-level almost remains flat between the (0, 1) and (1, 1) states, which is also expected from the measured spectra [see Figs. 5(c) and 5(d)].

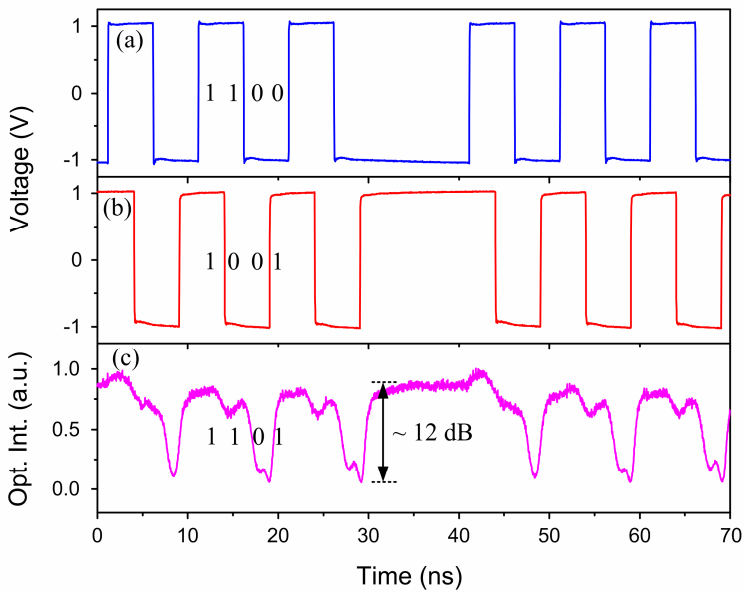

Fig. 6. (a). and (b). 200-Mbps NRZ electrical input data streams across nodes *A* and *B*. (c). Measured optical waveform at a probe wavelength near the resonance "*".

6. Conclusion

We experimentally demonstrated a silicon microring carrier-injection-based modulator with a cross-coupled U-bend waveguide. Both the microring and the cross-coupled waveguide were laterally integrated with p-i-n diodes. By applying a DC-bias either across the cross-coupled waveguide or the microring, we demonstrated resonance tuning with controlled extinction ratio exceeding 10 dB at an optimum bias voltage of the order of 1 V. Our experiments also suggested better modulator response from modulating the relatively long diode along the U-bend cross-coupled waveguide than from modulating the relatively short diode along the arcs of the microring. We also experimentally demonstrated silicon microring electrical-control OR-logic switching using the same device configuration with dual data inputs. Further theoretical modeling and measurements of the feedback-coupled microring resonance spectra are in progress and will be reported in a follow-up publication.

#80360 - $15.00 USD Received 22 Feb 2007; revised 9 Apr 2007; accepted 10 Apr 2007; published 11 Apr 2007

Acknowledgment

The research was substantially supported by a grant from the Research Grants Council of the Hong Kong Special Administrative Region, China (Project No. 618505).

#80360 - $15.00 USD Received 22 Feb 2007; revised 9 Apr 2007; accepted 10 Apr 2007; published 11 Apr 2007